Chemometrics and Intelligent Laboratory Systems 172 (2018) 188–193

Contents lists available at ScienceDirect

Chemometrics and Intelligent Laboratory Systems

journal homepage: www.elsevier.com/locate/chemometrics

Deep-learning-based regression model and hyperspectral imaging for rapid detection of nitrogen concentration in oilseed rape (*Brassica napus L.*) leaf

Xinjie Yu *, Huanda Lu, Qiyu Liu

Ningbo Institute of Technology, Zhejiang University, Ningbo 315100, China

ARTICLE INFO

Keywords:
Stacked auto-encoders
Fully-connected neural network
Deep learning
Nitrogen concentration
Oilseed rape
Nondestructive detection

ABSTRACT

Deep-learning-based regression model composed of stacked auto-encoders (SAE) and fully-connected neural network (FNN) was used for the detection and quantification of nitrogen (N) concentration in oilseed rape leaf. SAE was applied to extract deep spectral features from visible and near-infrared (380–1030 nm) hyperspectral image of oilseed rape leaf, and then these features were used as input data for FNN to predict N concentration. The SAE-FNN model achieved reasonable performance with $R^2_P = 0.903$, RMSEP =0 .307% and $RPD_P = 3.238$ for N concentration. Results confirmed the possibility of rapid and nondestructive detecting N concentration in oilseed rape leaf by the combination of hyperspectral imaging technique and deep learning method.

1. Introduction

Oilseed rape (*Brassica napus L.*) is one of the most important oil crops worldwide. In recent decades, a rapid increase in production of oilseed rape has required the improvement of fertilizer management to optimize the crop yield and product quality. Rapid detection of nitrogen (N) concentration in oilseed rape leaf during the growing season is essential to accurately manage the nitrogen fertilizer applications, which have great benefits in improving yield and quality of the oilseed rape crop [1].

Hyperspectral imaging (HSI) technique has recently emerged as the powerful tool for rapid and nondestructive detection of chemical properties (such as water, nitrogen, and nutrient levels) in plant [2]. It is of interest to further investigate if HSI has the potential for detecting the N concentration in oilseed rape leaf. However, as hyperspectral images are composed by hundreds of contiguous wavebands for each pixel of the object be measured, the problems of such huge number of data increase the data processing load, resulting in the complexity of spectral feature selection as well as chemometrical modeling. Thus, considering the high computational cost, the traditional chemometrical methods such as partial least square (PLS) regression, least-squares support vector machine (LS-SVM), and multi-linear regression (MLR) usually depend on calculating a mean spectrum from all pixels to reduce the data processing load. Unfortunately, in case of the analysis of a solid form sample like oilseed rape leaf, the use of a mean spectrum on a surface can be a drawback, since the mean spectrum cannot reveal global information in the hyperspectral image. So far, very little work has been done to apply a big data analysis on each pixel in the hyperspectral image (pixel-level spectra) for the detection of chemical properties in plants.

Deep learning [3], a deep architecture of artificial neural networks with capable of processing large scale data, has dramatically improved the state-of-the-art results in many different regression and classification tasks, which is expected to solve the above-mentioned problems caused by large scale data processing in hyperspectral images. In this study, a deep-learning-based regression model composed of stacked auto-encoders (SAE) [4] and simple fully-connected neural network (FNN) [5] is proposed for the detection of N concentration in oilseed rape leaf. The SAE is trained on pixel spectra in an unsupervised manner to automatically learn deep spectral features from hyperspectral image, and the deep spectral features are fed to the FNN to quantitatively predict the corresponding N concentration in a supervised manner.

2. Materials and methods

2.1. Sample preparation

Oilseed rapes (*B. napus, Zheyou51*) were planted in an experimental field of a local farm located in Ningbo, Zhejiang, China (30.32°N, 121.18°E). In order to produce different levels of N in leaves, four nitrogen levels including 0 (represented no nitrogen fertilizer), 100, 200 and 300 kg/ha^2 were applied, respectively, using urea as the nitrogen fertilizer. Eight experimental plots of 2.0 m × 1.5 m were used with two plots for each nitrogen level. Leaf sampling was carried out before the

* Corresponding author.
E-mail address: xjyu1979@nit.zju.edu.cn (X. Yu).

https://doi.org/10.1016/j.chemolab.2017.12.010
Received 22 October 2017; Received in revised form 1 December 2017; Accepted 18 December 2017
Available online 19 December 2017

ripe stage on 12 February, 9 March, 22 March, 8 April, and 26 April 2016. Four leaves at the same position in oilseed rape plants were selected randomly from each experimental plot, and were regarded as one sample. The collected leaves were sealed in plastic bags after being picked from the oilseed rape plant, and then taken to laboratory for hyperspectral image acquisition and chemical analysis of nitrogen concentration within 4 h. Finally, a total of 192 samples were acquired during the 2015–2016 growing season. In the experiments, 128 samples were randomly chosen out and used as calibration set for establishing regression models, whereas, the remaining 64 samples were used as prediction set for estimating the performance of regression models.

2.2. Measurements of N concentration

For each sample, whole leaves were used for the chemical analysis of N concentration. The leaves were placed into an oven to dry at 105 °C for half an hour, and then let cooled to 70 °C till a constant weight was recorded. The dry leaves were ground into fine powder. The powder of each sample was individually weighed, and then was used to measure nitrogen concentration by the Kjeldahl method after acid digestion. The N concentration (%) of leaf was calculated using the percentage of mg nitrogen per mg dry weight with accuracy of 0.001%.

2.3. Hyperspectral imaging system, image acquisition and correction

A laboratory visible and near infrared (VIS/NIR) hyperspectral imaging system composed of a spectrograph with working spectral range of 380–1030 nm and a CCD camera was used for the acquisition of hyperspectral images of oilseed rape leaves. The details of the main components of the system had been described in our former research work [6]. Before the measurement of N concentration, leaf was placed on a sample holder of the HSI system and then was scanned line by line at a constant moving speed of 4.5 mm s^{-1} and an exposure time of 16 ms of the CCD camera. The CCD camera used a two-dimensional detector array with 816 × 512 (spatial × spectral) mode to record the spectrum reflected from one line segment of the sample, and 600 lines were recorded for each sample to build a hyperspectral image (I_O) with dimension (x, y, λ), where x and y are the spatial dimensions (number of rows and columns in pixels) and λ is the number of spectral wavebands. The acquired hyperspectral images were then corrected according to the following equation:

$$I_C = \frac{I_O - B}{W - B} \times 100, \tag{1}$$

where I_C is the corrected hyperspectral image in a unit of relative reflectance (%), I_O is the original hyperspectral image, B is the black image (approximately 0% reflectance) recorded by closing completely the aperture of the camera, and W is the white image obtained by a white surface board with uniform, stable and high reflectance standard (approximately 99% reflectance).

2.4. Spectra extraction

After image correction, region of interest (ROI) of each sample was chosen manually from the corrected hyperspectral image using ENVI 5.0 (ITT Visual Information Solutions, Boulder, CO, USA) software. The ROI selection was based upon the whole area of leaf that was used for determination of N concentration. For each sample, spectral data in the range of 380–1030 nm wavelength with 512 bands of each pixel within the ROI were extracted, then averaged at each wavelength variable to obtain a mean spectrum representing one sample. Meanwhile, in order to create a big data set for deep learning, 800 pixel spectra data were randomly selected out from the ROI for each sample. The extracted random pixel spectra were used to train deep-learning-based SAE-FNN model, while the mean spectra were used to train traditional methods such as PLSR and LS-SVM.

2.5. SAE-FNN regression model for N concentration

A deep-learning-based regression model consisting of stacked auto-encoders and fully-connected neural network (denoted as SAE-FNN) was established for the prediction of N concentration in oilseed rape leaf. The SAE-FNN is a deep neural network architecture, in which SAE is used as an unsupervised manner to extract deep spectral features and FNN is used as a supervised manner to predict target chemical concentration based on the corresponding deep spectral features.

The SAE consist multiple layers of auto-encoder [7], which aims to extract the non-linear features from input data. The auto-encoder has one input layer of d units, one hidden layer of h units, one output layer of d units, and an activation function$f(\cdot)$. During learning, it first maps the input $x \in R^d$ to the hidden layer and produces the latent activity$y \in R^h$, which is called "encoding". Then, y is mapped back to an output (reconstructed) layer that has the same size of the input layer, which is called "decoding". The reconstructed values are denoted as$z \in R^d$. These two steps can be formulated as:

$$y = f\left(w_y x + b_y\right), \tag{2}$$

$$z = f(w_z y + b_z), \tag{3}$$

where w_y is the input-to-hidden weight matrix, $w_z$is the hidden-to-output weight matrix, b_y and b_z denote the bias of hidden and output units, and $f(\cdot)$ denotes the activation function. In our experiments, "leaky-ReLU" non-linearity function [8] was considered for the activation function$f(\cdot)$, and the following constraint holds

$$w_y = w'_z = W. \tag{4}$$

The goal of learning is to minimize the "error" between input and output (reconstructed input), which are denoted as:

$$\underset{W,b_y,b_z}{\operatorname{argmin}}[c(x,z)], \tag{5}$$

where z is reconstructed data which dependent on parameters W, b_y, b_z , while x is given input. Since the auto-encoder can reproduce input data x at reconstructed data z by hidden representation $y$in an unsupervised way, the values in the y can then be employed as reduced feature variables representing the original input x. The auto-encoders can be stacked to build SAE, which can produce better high-level features compared to the single layer auto-encoder. Therefore, in this study, we used SAE to extract deep spectral features from hyperspectral image, and then these features were used as input data for FNN to predict N concentration.

For the prediction purpose, the decoding part of SAE is removed and the encoding part of SAE is retained, then a FNN is added to the last encoding layer of SAE to produce a SAE-FNN regression model. The SAE-FNN includes SAE pre-training and FNN fine-tuning. SAE pre-trains the network weights (deep spectral features) by using random pixel spectra as input data, and the learned weights (deep spectral features) acted as the initial weights of the SAE-FNN network. Further, FNN is used to fine-tune the whole SAE-FNN network weights by using the mean spectra and the corresponding chemical measured N concentrations as input data. The FNN is a fully-connected back propagation neural network. No activation function is used for the output layer of FNN network because it is a regression problem, and the output of FNN is a single unit denoted as:

$$\widehat{Y} = w_l y_l + b_l, \tag{6}$$

where $\widehat{Y}$is the output numerical value (predicted N concentration), w_l is the weight matrix, b_l denote the bias of output unit, and y_l is the outputs of the last encoding layer which are also the deep feature variables pre-trained by SAE.

We can use the errors between the predicted N concentration results and the chemical measured N concentrations associated with the training

mean spectra to fine-tune the whole SAE-FNN network weights in a supervised manner. The loss function for back propagation of SAE-FNN is defined as the following mean squared error (MSE) function:

$$MSE = \frac{1}{n}\sum_{i=1}^{n} \widehat{Y}_i - Y_i^2, \quad (7)$$

where n is the total number of training mean spectra sample, Y_i is the chemical measured N concentration of sample i, and $\widehat{Y}_i$ is the corresponding predicted N concentration. The optimization problem of minimizing the MSE loss function is solved by "adam" optimizer [9].

The SAE–FNN modeling was conducted on a windows 7 system with an Intel i7-4510U processor, which has 2 cores of 2.6 GHz. The SAE–FNN algorithm was carried out using Keras which is a python language based framework for deep learning and can use GPU to speed up the calculation for large scale dataset [10]. In the experiments, we use a GPU of NVIDIA GT720 M to make the training procedure faster.

On the other hand, traditional methods including PLS and LS-SVM with nonlinear radial basis function (RBF) kernel were also applied to establish regression models for N concentration, and their performances were compared with that of SAE-FNN. The PLS algorithm was carried out using a PLS-regression function in the machine learning framework of Scikit-learn [11]. The LS-SVM was executed in the MATLAB 8.1 (The Math Works, Natick, USA) using a LS-SVM toolbox (available at http://www.esat.kuleuven.be/sista/lssvmlab/).

2.6. Model evaluation

The performances of PLS, LS-SVM and SAE-FNN regression models were evaluated against the following standards: coefficient of determination in calibration (R^2_C) and prediction (R^2_P), root mean square error (RMSE) of calibration (RMSEC) and prediction (RMSEP), as well as residual predictive deviations (RPD_c, RPD_p) that were calculated by dividing the standard deviation (SD) of the reference values by RMSEC and RMSEP, respectively. Generally, a good model should yield high values of RPD_C, RPD_P, R^2_C, R^2_P, while low values of RMSEC, RMSEP, as well as a small difference between them.

3. Results and discussion

3.1. Chemical measurement results of N concentration

The chemical measurement results showed that a relatively high variability was appeared in N concentrations. For all 192 measured oilseed rape leaf samples, the N concentrations ranged from 2.834% to 6.294% with a mean value of 4.630% and a standard deviation of 1.018%. This relatively high variability appeared in N concentrations is because of the different N levels of fertilization design, different growing stages and different leaf positions the samples were collected from. For the calibration modeling purpose, all samples were randomly divided into calibration set of 128 samples and prediction set of 64 samples. The N concentrations ranged from 2.834% to 6.294% for the samples in calibration set, and 3.011%–6.210% for the samples in prediction set, respectively. It should be noted that a wide range of data variability in the reference measurement is help to the building of robust models while a narrow range of variability can negatively affect predictability of any chemical attributes.

3.2. Spectral characteristics of oilseed rape leaves

The reflectance mean spectra of samples with different N concentrations (2.872%, 3.797% and 4.987%) are illustrated in Fig. 1. The vibrations appeared in the VIS region around 550 nm is caused by chlorophyll, which related to N concentrations in plant leaf. The region of 670–760 nm with rapid changed reflectance is well known as the "red edge" of plant in the electromagnetic spectrum, which can be used as a potential index for detecting differences in plant nitrogen status. Some small peaks observed in the range of 760–980 nm are mostly attributed to the overtones of O-H functional groups related to water in leaf, as well as the overtones of N-H functional groups related to nitrogen in leaf [12]. The above differences in the spectral characteristics of leaves indicated that hyperspectral imaging had the potential to discriminate oilseed rape leaves with different N concentrations.

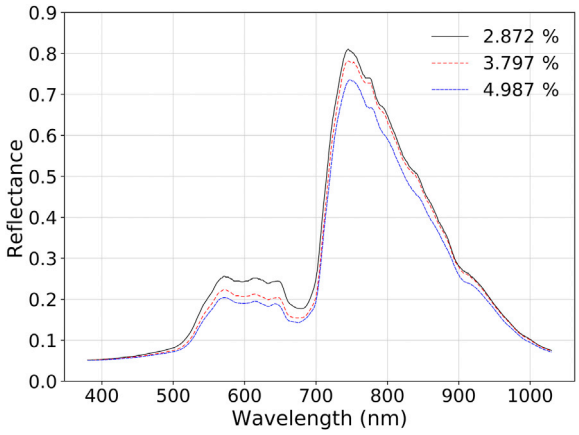

Fig. 1. Mean spectra from the hyperspectral images of oilseed rape leaf samples with different N concentrations.

3.3. Regression analysis using PLS

PLS was applied to establish regression model for N concentration by using the mean spectra in the calibration set. The number of latent variables (LVs) was optimized as 6 under full cross validation for PLS model. The performance of the PLS model for N concentration in both calibration and prediction sets is displayed in Table 1. The PLS model obtained a result for predicting N concentration with the values of R^2_P, RMSEP and RPD_P were 0.854, 0.377% and 2.637 for prediction set. According to the standard for evaluating the regression models, the value of R^2 in the range of 0.82–0.90 usually indicates good performance, and higher than 0.90 shows excellent performance; a RPD value greater than 2.0 indicates a good quantitative model, while larger than 3.0 means that the model is excellent [13]. The established PLS model showed good performance with R^2_P>.82 and RPD_P>2.0 for N concentration in oilseed rape leaf, showing that the model can be used for practical applications.

The correlation between the mean spectral wavebands and N concentration was analyzed by using the weighted regression coefficients of

Table 1
Calibration and prediction results of the N concentration in oilseed rape leaf using different regression models.

Model	Calibration set			Prediction set		
	R^2_C	RMSEC (%)	RPD_C	R^2_P	RMSEP (%)	RPD_P
PLS	0.922	0.288	3.590	0.854	0.377	2.637
LS-SVM	0.945	0.241	4.290	0.876	0.347	2.865
SAE-FNN5	0.929	0.274	3.774	0.849	0.383	2.595
SAE-FNN10[a]	**0.952**	**0.225**	**4.596**	**0.903**	**0.307**	**3.238**
SAE-FNN20	0.954	0.221	4.679	0.895	0.320	3.106
SAE-FNN30	0.964	0.195	5.303	0.887	0.331	3.003
SAE-FNN40	0.950	0.229	4.515	0.883	0.338	2.940
SAE-FNN50	0.967	0.188	5.500	0.865	0.362	2.746
SAE-FNN60	0.964	0.196	5.276	0.876	0.348	2.856
SAE-FNN70	0.964	0.195	5.303	0.820	0.420	2.367
SAE-FNN80	0.977	0.158	6.544	0.901	0.311	3.196
SAE-FNN90	0.957	0.213	4.854	0.858	0.372	2.672

[a] The number of 10 represents the units of the last layer (deep spectral features) in SAE encoding part. The row with bold style shows the best performance for the prediction of N concentration.

the optimized 6 LVs in PLS model. As shown in Fig. 2, whereas the reflectance near 530, 700 and 750 nm have high positive correlations, those near 670, 720, 790 and 840 nm have high negative correlations with the N concentrations. The above seven wavebands are closely related with the N attributes in oilseed rape plant, which is consistent with the results of spectral characteristics that have been analyzed in the "spectral characteristics of oilseed rape leaves" section. Therefore, according to the above results, it can be safely confirmed that hyperspectral image on the spectral range (380–1030 nm) was feasible to rapidly determine N concentration in oilseed rape leaf.

3.4. Regression analysis using LS-SVM

LS-SVM was also applied to build a regression model based upon the mean spectra for the prediction of N concentration in oilseed rape leaf. The optimal parameters of γ and σ^2 were achieved with $\gamma = 9.554 \times 10^4$ and $\sigma^2 = 3.291 \times 10^4$ for the LS-SVM model. The calibration and prediction results of LS-SVM model for N concentrations are showed in Table 1. The LS-SVM slightly superior to PLS in both calibration and prediction sets. Here, the values of R^2_C, RMSEC and RPD_C were 0.945, 0.241% and 4.290 for calibration set, and the values of R^2_P, RMSEP and RPD_P were 0.876, 0.347% and 2.865 for prediction set, respectively. This better performance of LS-SVM model can also be observed in the plots of measured vs. predicted N concentration that are displayed in Fig. 3. By comparing the compactness of samples around the regression line in Fig. 3, LS-SVM model (Fig. 3b) is found to be with higher correlation coefficient of measured values and predicted values than that of PLS (Fig. 3a).

Although the above results indicated that the performance for the prediction of N concentration was improved by LS-SVM, the slightly increased value of 0.022 for R^2_P was still not significant. Recent studies have reported that deep learning method play a positive role in regression task and can improve the generalization performance of models in many applications. Thus, in the next section, deep learning method was conducted to establish regression model to investigate if it was possible to further increase prediction accuracy for N concentration in oilseed rape leaf.

3.5. Regression analysis using SAE-FNN

SAE-FNN was established to predict N concentration in oilseed rape leaf. In our work, 800 randomly selected pixel spectra together with one mean spectrum for each sample in the calibration set (a total of 102,528 spectra) were considered as big dataset to pre-train the SAE in an unsupervised way. The pre-training was carried out under a SAE with symmetric seven-hidden-layer structure. The numbers of units in the seven layers of the SAE were set as 512, 220, 100, *h*, 100, 220 and 512, where *h* represented the units of the last layer (deep spectral features) in the encoding part of SAE. An example of the pre-training result of SAE with $h = 10$ is displayed in Fig. 4. Here, when the SAE is trained with 100 iterating epochs, the average validation error between the original input spectra and the reconstructed output spectra tends to be a very small value of 0.132×10^{-4} (Fig. 4a), indicating that the SAE can perfectly reproduce the original input spectra (Fig. 4b) at reconstructed spectra (Fig. 4f). Spectral features of the oilseed rape leaves with different N concentrations are calculated from first, second and last layers in the encoding part of SAE, and are illustrated as curves in Fig.4c-e. It can be observed that the spectral features become more abstract as the number of units in the encoding layers reducing from 220 to 10. These reduced feature variables carry the most valuable information representing the original spectra of oilseed rape leaves, and may help to build a robust regression model for N concentration. As the units number of the last encoding layer (*h*) in SAE always play an important role in the accuracy of regression models, we pre-trained a series of SAEs by varying the *h* chosen from [5, 10, 20, 30, 40, 50, 60, 70, 80, 90], and obtained the optimal number according to the prediction results of N concentration using the corresponding SAE-FNN model.

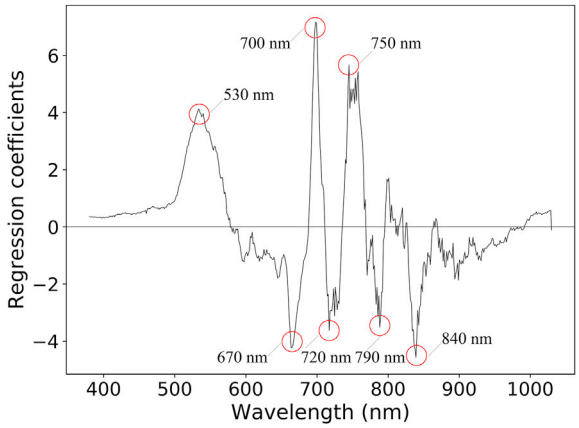

Fig. 2. Regression coefficients between spectral reflectance and N concentration.

For the prediction of N concentration, decoding part of the pre-trained SAE was removed and encoding part was retained, then a FNN layer was added to the last encoding layer to produce a SAE-FNN regression model for N concentration. The pre-trained weights of the encoding part of SAE acted as the initial weights of the SAE-FNN model. 128 mean spectra with measured N concentrations in the calibration set were used to fine-tune the whole SAE-FNN regression model in a supervised manner, while the remain 64 samples in the prediction set were used as unknown samples to evaluate the performance of the fine-tuned SAE-FNN regression model. In our experiments, SAEs were pre-trained with a batch size of 100 and an epoch value of 100, and SAE-FNN models were fine-tuned with a batch size of 100 and an epoch value of 11,000.

The performances of SAE-FNN regression models with different deep spectral features (expressed as SAE-FNN5, SAE-FNN10, SAE-FNN20, SAE-FNN30, SAE-FNN40, SAE-FNN50, SAE-FNN60, SAE-FNN70, SAE-FNN80 and SAE-FNN90) are listed in Table 1. All ten SAE-FNN models produced good results with $R^2_P > .82$ and $RPD_P > 2.0$, further proving that the VIS/NIR hyperspectral imaging technology was suitable for the prediction of N concentration in oilseed rape leaf. Moreover, five SAE-FNN models (SAE-FNN10, SAE-FNN20, SAE-FNN30, SAE-FNN40 and SAE-FNN80) achieved better results than those yielded by PLS and LS-SVM models. The best result for N concentration was obtained by the SAE-FNN10 model with $R^2_C = 0.952$, RMSEC = 0.225%, $RPD_C = 4.596$ for calibration set, and $R^2_P = 0.903$, RMSEP = 0.307%, $RPD_P = 3.238$ for prediction set, respectively. The values of and $R^2_P = 0.903$ and $RPD_P = 3.238$ in the SAE-FNN10 model showed that the established model was reasonable (with $R^2_P > 9.0$ and $RPD_P > 3.0$) for N concentration prediction. This superiority of the SAE-FNN method can also be confirmed by the high correlation coefficient of measured values and predicted values of SAE-FNN10 model displayed in Fig. 3c.

The obtained results of SAE-FNN models indicate that deep learning can increase the prediction accuracy for N concentration in oilseed rape leaf. This phenomenon could be explained by following reasons. Firstly, the hyperspectral data of oilseed rape leaves are very complicated and tend to nonlinearity due to various undesired effects such as multi-scattering in the acquisition process, inhomogeneous samples, environmental changes, and instrumental variations. In our works, the pre-training of SAE acted as a highly efficient non-linear data dimension reduction method which can capture non-linear deep spectral features from hyperspectral image by training deep neural networks. This might result in improved efficacy of spectral feature extraction and prediction accuracy for N concentration of oilseed rape leaf. Secondly, large amounts of training data might be effective in avoiding over-fitting as well as improving generalization performance for both regression and classification task. Our deep-learning-based SAE-FNN regression model

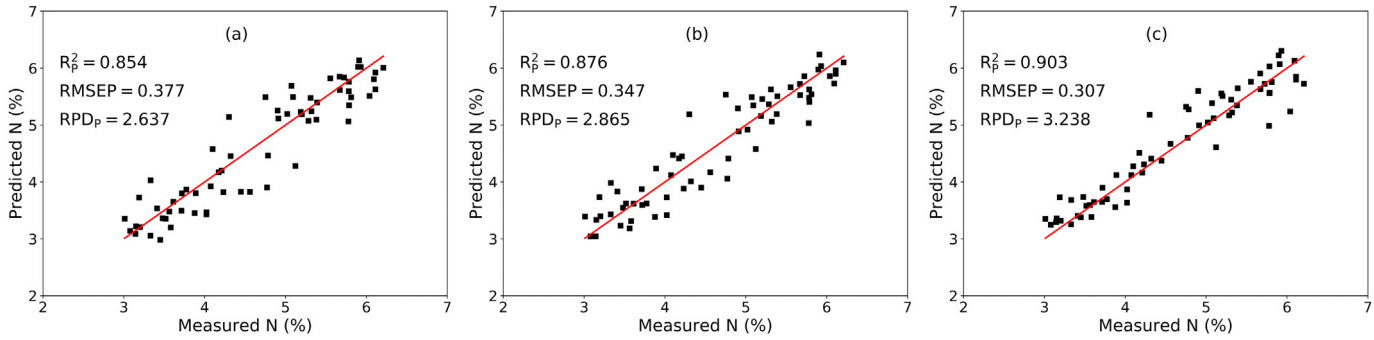

Fig. 3. Measured vs.predicated N concentrations for oilseed rape leaves by the regression models of PLS (a), LS-SVM (b) and SAE-FNN10(c).

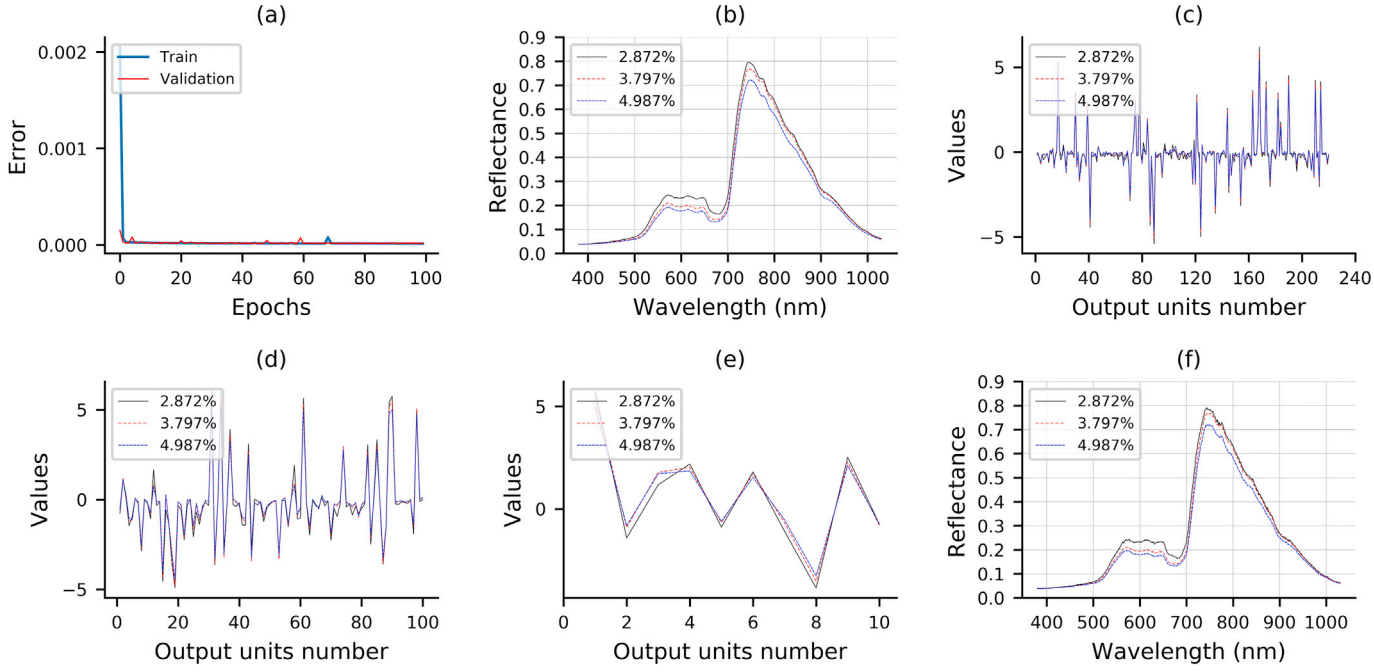

Fig. 4. The pre-training result of a SAE.Reconstruction error of training (a), original input spectra curves (b), deep spectral features of first, second and last layer in the encoding part of SAE(c)-(e), and reconstructed output spectra curves(f).

was obtained by pre-training SAE on a very large number of random pixel spectra, which help to revealing global information in the hyperspectral data for N concentration prediction. Hence, the performances of SAE-FNN models were higher than those of PLS and LS-SVM models.

4. Conclusions

The results of this study demonstrate that deep learning was feasible to be used as HSI data analysis method for N prediction in oilseed rape leaf. SAE-FNN model based upon 10 deep spectral features gave reasonable accuracy for the prediction of N concentration in oilseed rape leaf with $R^2_C = 0.952$, RMSEC = 0.225%, $RPD_C = 4.596$, and $R^2_P = 0.903$, RMSEP = 0.307%, $RPD_P = 3.238$. To the best of our knowledge, this is the first time deep learning algorithm is applied to the nutrient inspection of oilseed rape plant. The results obtained by the SAE-FNN method would encourage more research efforts on using the deep learning as a novel chemometrical method for nutrient detection of plant.

Acknowledgement

The research leading to these results has received funding from the Zhejiang Provincial Natural Science Foundation of China (no.LY15C190011), the National Natural Science Foundation of China (no.31201446 and no.31402352), the Ningbo Science and Technology Special Project of China (no.2017C110002), the Ningbo People's Livelihood Science and Technology Project of China (no.2013C11026), the Scientific Research Project of Zhejiang Education Department (no.Y201738720) and the Ningbo Natural Science Foundation (no.2015A610131).

References

[1] F. Wang, J. Huang, Y. Wang, Z. Liu, F. Zhang, Estimating nitrogen concentration in rape from hyperspectral data at canopy level using support vector machines, Precis. Agric. 14 (2013) 172–183.
[2] P. Pandey, Y. Ge, V. Stoerger, J.C. Schnable, High throughput in vivo analysis of plant leaf chemical properties using hyperspectral imaging, Front. Plant Sci. (2017). https://doi.org/10.3389/fpls.2017.01348.
[3] Y. LeCun, Y. Bengio, G.E. Hinton, Deep learning, Nature 521 (2015) 436–444.
[4] J. Zabalza, J. Ren, J. Zheng, H. Zhao, C. Qing, Z. Yang, P. Du, S. Marshall, Novel segmented stacked autoencoder for effective dimensionality reduction and feature extraction in hyperspectral imaging, Neurocomputing 185 (2016) 1–10.
[5] C.R. Gent, C.P. Sheppard, Special Feature. Predicting time series by a fully connected neural network trained by back propagation, Comput. Contr. Eng. J. 3 (1992) 109–112.
[6] X. Yu, L. Tang, X. Wu, H. Lu, Nondestructive freshness discriminating of shrimp using visible/near-infrared hyperspectral imaging technique and deep learning algorithm, Food Anal. Meth (2017). https://doi.org/10.1007/s12161-017-1050-8.

[7] C. Tao, H. Pan, Y. Li, Z. Zou, Unsupervised spectral–spatial feature learning with stacked sparse autoencoder for hyperspectral imagery classification, IEEE Geosci. Remote Sens. Lett. 12 (2015) 2438–2442.
[8] X.Y. Zhang, Y. Bengio, C.L. Liu, Online and offline handwritten Chinese character recognition: a comprehensive study and new benchmark, Pattern Recogn. 61 (2017) 348–360.
[9] K. Gopalakrishnan, S.K. Khaitan, A. Choudhary, A. Agrawal, Deep convolutional neural networks with transfer learning for computer vision-based data-driven pavement distress detection, Construct. Build. Mater. 157 (2017) 322–330.
[10] F. Chollet, Keras: theano-based deep learning library. Code. https://github.com/fchollet, 2015. (Accessed 25 September 2017). http://keras.io.
[11] F. Pedregosa, G. Varoquaux, A. Gramfort, V. Michel, B. Thirion, O. Grisel, M. Blondel, P. Prettenhofer, R. Weiss, V. Dubourg, J. Vanderplas, A. Passos, D. Cournapeau, M. Brucher, M. Perrot, É. Duchesnay, Scikit-learn: machine learning in python, J. Mach. Learn. Res. 12 (2011) 2825–2830.
[12] M. Corti, P.M. Gallina, D. Cavalli, G. Cabassi, Hyperspectral imaging of spinach canopy under combined water and nitrogen stress to estimate biomass, water, and nitrogen content, Biosyst. Eng. 158 (2017) 38–50.
[13] R.A. Viscarra Rossel, R.N. McGlynn, A.B. McBratney, Determining the composition of mineral-organic mixes using UV-vis-NIR diffuse reflectance spectroscopy, Geoderma 137 (2006) 70–82.